Dissipative particle dynamics: Bridging the gap between atomistic and mesoscopic simulation

2 authors, including:

Rob Groot
Unilever, Vlaardingen, Netherlands
56 PUBLICATIONS **9,789** CITATIONS

Dissipative particle dynamics: Bridging the gap between atomistic and mesoscopic simulation

Robert D. Groot and Patrick B. Warren

Unilever Research Port Sunlight Laboratory, Quarry Road East, Bebington, Wirral, L63 3JW, United Kingdom

We critically review dissipative particle dynamics (DPD) as a mesoscopic simulation method. We have established useful parameter ranges for simulations, and have made a link between these parameters and χ-parameters in Flory-Huggins-type models. This is possible because the equation of state of the DPD fluid is essentially quadratic in density. This link opens the way to do large scale simulations, effectively describing millions of atoms, by firstly performing simulations of molecular fragments retaining all atomistic details to derive χ-parameters, then secondly using these results as input to a DPD simulation to study the formation of micelles, networks, mesophases and so forth. As an example application, we have calculated the interfacial tension σ between homopolymer melts as a function of χ and N and have found a universal scaling collapse when $\sigma/\rho k_B T \chi^{0.4}$ is plotted against χN for $N>1$. We also discuss the use of DPD to simulate the dynamics of mesoscopic systems, and indicate a possible problem with the timescale separation between particle diffusion and momentum diffusion (viscosity). © *1997 American Institute of Physics.* [S0021-9606(97)51335-3]

I. INTRODUCTION

Many systems of academic and industrial interest are examples of soft condensed matter: They are neither completely solid nor completely liquid. When we take a closer look at the background of these systems a common feature arises, namely the existence of a relevant length-scale in between the atomistic scale and the macroscopic scale. In some cases, when we consider polymer gels, this length-scale is set by the distance between the cross-links in the gel. Simulation on this length-scale, using a simple bead-and-spring model has proved appropriate to analyze the phase diagram and the rheology.[1] Surprisingly, the linear viscoelastic behavior that results from this model shows a universal behavior similar to what is found in many experimental systems[2] even without the incorporation of hydrodynamic interactions. This in itself indicates that for polymer gels the nature of the chemistry is not important, but life-time and structure of the polymer connections is.[3]

If we now draw attention to other types of systems, where surfactant mesophases form the structuring mechanism, a similar universality is found. In this case the flexibility or bending rigidity of a lamellar bilayer leads to a mesoscopic length-scale: the wavelength of undulations of the lamellar sheets.[4] The precise value of the rigidity of bilayers is a subject of debate, and by no means trivial.[5] However, an analysis in terms of lamellar sheets presupposes their existence, whereas in reality many self assembled structures can occur.[6,7] The available techniques to predict these phases range from Monte Carlo methods of lattice polymers,[8] self-consistent field theory,[9] to dynamic density functional theory.[10] A problem with these techniques is that they all describe polymers confined to lattice conformations, and are not very well suited to describe branched polymers. Multiblock copolymers and branched polymers are molecules that are capable of forming lamellar structures (or more general mesostructures), and are candidates to form weak gels. Some polymer zones may form micelles, and if these micelles are connected by polymer strings a network is formed.

Although the behavior of these networks on larger length-scales is now reasonably well understood, we still cannot make the full connection from atomistic length-scale to the macroscopic world. In simulations of associative liquids[1,2] the associated atoms are moved together as one new species. This implies that the order of association is defined at forehand (in this case binary association). Consequently, properties defined on a smaller length-scale than an effective cross-link, like how many chains are joined together in a micelle, cannot be predicted. Furthermore, hydrodynamic interactions are not accounted for. To bridge the gap between atomistic simulations and these large scale network simulations, we therefore seek an intermediate simulation technique aimed at a length-scale larger than the atomistic scale, but smaller than the network connection scale.

A few years ago Hoogerbrugge and Koelman introduced a new simulation technique for hydrodynamic behavior, called dissipative particle dynamics (DPD).[11,12] This technique is based on the simulation of soft spheres, whose motion is governed by certain collision rules. By introducing bead-and-spring type particles, polymers can be simulated with the same method.[13,14] As applications of the method abound, it is necessary to create a firm basis from which we can interpret what the simulation means, before we go into any detail on the results of the simulations. The aim of the present article is to provide such an interpretation. The starting point of this analysis will be the formulation of DPD by Español and Warren,[15] who studied the fluctuation-dissipation theorem in connection with this method. In their formulation all particles interact by three forces: a conserva-

tive force $\mathbf{F}^C$, a dissipative force $\mathbf{F}^D$, and a random force $\mathbf{F}^R$. They showed that the dissipative force and the random force have to satisfy a certain relation in order that the system has the statistical mechanics corresponding to the canonical ensemble with a temperature related to the relative amplitudes of the random and dissipative interactions.

In the present article the physical interpretation of this relation is discussed, and algorithms formulated for arbitrary timesteps. The negative consequences of not satisfying this relation are elucidated, and the statistical mechanical validity of the method is checked explicitly as a function of the timestep size. Once the validity is established, the thermodynamic basis of the model is investigated. A simple scaling relation is found, which leads to the interpretation of the underlying model in terms of the well known Flory-Huggins theory of polymers. This opens the way to bridge the gap from atomistic simulations, where solubility parameters can be calculated, to mesoscopic simulations where mesophases and network formation can be studied. Finally, as an example of a practical application, we examine the surface tension between homopolymer melts.

II. THE DPD SIMULATION METHOD

A set of interacting particles is considered, whose time evolution is governed by Newton's equations of motion

$$\frac{d\mathbf{r}_i}{dt} = \mathbf{v}_i, \quad \frac{d\mathbf{v}_i}{dt} = \mathbf{f}_i. \tag{1}$$

For simplicity the masses of the particles are put at 1, so that the force acting on a particle equals its acceleration. The force contains three parts, each of which is pairwise additive:

$$\mathbf{f}_i = \sum_{j \neq i} (\mathbf{F}_{ij}^C + \mathbf{F}_{ij}^D + \mathbf{F}_{ij}^R), \tag{2}$$

where the sum runs over all other particles within a certain cutoff radius r_c. As this is the only length-scale in the system, we use the cutoff radius as our unit of length, $r_c = 1$. The conservative force is a soft repulsion acting along the line of centres and is given by

$$\mathbf{F}_{ij}^C = \begin{cases} a_{ij}(1 - r_{ij})\hat{\mathbf{r}}_{ij} & (r_{ij} < 1) \\ 0 & (r_{ij} \geq 1) \end{cases}, \tag{3}$$

where a_{ij} is a maximum repulsion between particle i and particle j; and $\mathbf{r}_{ij} = \mathbf{r}_i - \mathbf{r}_j$, $r_{ij} = |\mathbf{r}_{ij}|$, $\hat{\mathbf{r}}_{ij} = \mathbf{r}_{ij}/|\mathbf{r}_{ij}|$. The remaining two forces are a dissipative or drag force and a random force. They are given by

$$\mathbf{F}_{ij}^D = -\gamma w^D(r_{ij})(\hat{\mathbf{r}}_{ij} \cdot \mathbf{v}_{ij})\hat{\mathbf{r}}_{ij}, \quad \mathbf{F}_{ij}^R = \sigma w^R(r_{ij})\theta_{ij}\hat{\mathbf{r}}_{ij}, \tag{4}$$

where w^D and w^R are r-dependent weight functions vanishing for $r > r_c = 1$, $\mathbf{v}_{ij} = \mathbf{v}_i - \mathbf{v}_j$, and $\theta_{ij}(t)$ is a randomly fluctuating variable with Gaussian statistics: $\langle \theta_{ij}(t) \rangle = 0$ and $\langle \theta_{ij}(t)\theta_{kl}(t') \rangle = (\delta_{ik}\delta_{jl} + \delta_{il}\delta_{jk})\delta(t - t')$. These forces also act along the line of centres and conserve linear and angular momentum. There is an independent random function for each *pair* of particles.

Español and Warren[15] showed that one of the two weight functions appearing in Eq. (4) can be chosen arbitrarily and that this choice fixes the other weight function. There is also a relation between the amplitudes and $k_B T$. In summary

$$w^D(r) = [w^R(r)]^2, \quad \sigma^2 = 2\gamma k_B T. \tag{5}$$

As a simple choice we take

$$w^D(r) = [w^R(r)]^2 = \begin{cases} (1 - r)^2 & (r < 1) \\ 0 & (r \geq 1) \end{cases} \tag{6}$$

(i.e., $w^R(r)$ is the same function as in the conservative force). Unlike Hoogerbrugge and Koelman[11] we choose not to include normalization factors in these functions.

In previous studies[11,15] a simple, Euler-type algorithm was used to advance the set of positions and velocities. For an arbitrary timestep it is found by integrating the equations of motion over a short interval of time Δt over which neither the positions nor velocities of particles change very much. This algorithm is

$$\mathbf{r}_i(t + \Delta t) = \mathbf{r}_i(t) + \Delta t \mathbf{v}_i(t),$$

$$\mathbf{v}_i(t + \Delta t) = \mathbf{v}_i(t) + \Delta t \mathbf{f}_i(t), \tag{7}$$

$$\mathbf{f}_i(t + \Delta t) = \mathbf{f}_i(\mathbf{r}(t + \Delta t), \mathbf{v}(t + \Delta t)).$$

Care must be taken with the random force which becomes

$$\mathbf{F}_{ij}^R = \sigma w^R(r_{ij}) \zeta_{ij} \Delta t^{-1/2} \hat{\mathbf{r}}_{ij}, \tag{8}$$

where ζ_{ij} is a random number with zero mean and *unit* variance, again chosen independently for each *pair* of interacting particles and at each timestep. The appearance of $\Delta t^{-1/2}$ in this expression will be discussed below.

Rather than using the Euler algorithm as utilized by previous authors[11,15] in the context of DPD, a modified version of the velocity-Verlet algorithm[16] is used here:

$$\mathbf{r}_i(t + \Delta t) = \mathbf{r}_i(t) + \Delta t \mathbf{v}_i(t) + \frac{1}{2}(\Delta t)^2 \mathbf{f}_i(t),$$

$$\tilde{\mathbf{v}}_i(t + \Delta t) = \mathbf{v}_i(t) + \lambda \Delta t \mathbf{f}_i(t),$$

$$\mathbf{f}_i(t + \Delta t) = \mathbf{f}_i(\mathbf{r}(t + \Delta t), \tilde{\mathbf{v}}(t + \Delta t)), \tag{9}$$

$$\mathbf{v}_i(t + \Delta t) = \mathbf{v}_i(t) + \frac{1}{2}\Delta t (\mathbf{f}_i(t) + \mathbf{f}_i(t + \Delta t)).$$

If the force were independent of velocity, the actual velocity-Verlet algorithm would be recovered for $\lambda = 1/2$. Because the force does depend on velocity, we make a prediction for the new velocity, which we denote by $\tilde{\mathbf{v}}$, and correct for this afterwards in the last step. In this more sophisticated algorithm, the force is still updated once per iteration (after the second step) thus there is virtually no increase in computational cost. All physical measurements that depend on coordinate differences are also taken after the second step; the temperature is measured after the last step.

If there were no random or dissipative force, this algorithm would be exact to $O(\Delta t^2)$ at $\lambda = 1/2$. Because of the stochastic nature of the process, the order of the algorithm becomes unclear; this is discussed more fully by Öttinger,

for example.[17] The variable factor λ, introduced empirically, appears to account for some of the additional effects of the stochastic interactions. In practice, all simulations reported in this paper were carried out with $\lambda = 1/2$ with the exception of some investigations of the effect of λ on the steady state temperature reported in the next section.

The factor $\Delta t^{-1/2}$ appearing in the expression for the random force in Eq. (8) will now be discussed. It can be derived by integration of the underlying stochastic differential equations and interpreting the random force as a Wiener process,[18] but a heuristic argument as to why $\Delta t^{-1/2}$ appears is useful for a correct understanding of the method. Consider therefore the motion of a particle in a liquid over a fixed time-span. Due to collisions with other particles, a random force $f(t)$ acts on the particle. The mean value of this force is zero, but its variance is non-zero. To calculate this we divide the time axis in N intervals. In each of these intervals suppose the force has a random value f_i with zero mean $\langle f_i \rangle = 0$ and variance $\langle f_i^2 \rangle = \sigma^2$, where, initially, we suppose the variance has no dependence on the timestep. We will find that this leads to unphysical behavior. The random force is uncorrelated between different timesteps: $\langle f_i f_j \rangle = 0$ if $i \neq j$. The time-integral of the force is the momentum change of the particle. Since this is, up to a friction factor, equal to the displacement (the random force induces a random walk) the mean square value of the time integral of the force must be proportional to the square distance travelled in a diffusive process, i.e., proportional to time

$$
\langle F^2 \rangle = \left\langle \left(\int_0^t f(t')dt' \right)^2 \right\rangle
$$

$$
= \left\langle \left(\sum_{i=1}^N f_i \right)^2 \left(\frac{t}{N} \right)^2 \right\rangle = \sigma^2 t^2 / N = t \times \sigma^2 \Delta t. \quad (10)
$$

As the number of intervals N increases (i.e., $\Delta t = t/N$ decreases) this average would go to zero if, as initially assumed, $\langle f_i^2 \rangle$ is independent of Δt. As the mean diffusion over any physical time-interval must have a finite value that is independent of the stepsize of the integration, we must conclude that in actuality $\langle f_i^2 \rangle = \sigma^2 / \Delta t$ is appropriate. Thus the spread of the random force increases as we divide a given physical time interval up in more and more timesteps. This step-size dependence of the random force is precisely generated by the factor of $\Delta t^{-1/2}$ in Eq. (8).

At this point the reader may wonder why it is so important that Eq. (5) relating the dissipative and noise weight functions is satisfied. To answer this question, consider the distribution function $\rho(\mathbf{r}_i, \mathbf{p}_i, t)$, which gives the probability of finding the system in a state where the particles have positions $\mathbf{r}_i$ and momenta $\mathbf{p}_i$, at any particular time t. The time evolution of this distribution is governed by the Fokker-Planck equation derived by Español and Warren[15]

$$
\frac{\partial \rho}{\partial t} = \mathcal{L}^C \rho + \mathcal{L}^D \rho, \quad (11)
$$

where $\mathcal{L}^C$ and $\mathcal{L}^D$ are evolution operators that can be extracted from the time-evolution governing the motion of the

particles. The first is the Liouville operator of the Hamiltonian system interacting with conserved forces $\mathbf{F}^C$, the second operator $\mathcal{L}^D$ contains the dissipative and noise terms. Now if the dissipative and random forces are put at zero, we are left with a Hamiltonian system. In the canonical ensemble, the Gibbs-Boltzmann distribution $\rho^{eq}(\mathbf{r}_i, \mathbf{p}_i) = \exp(-\Sigma_i \mathbf{p}_i^2 / 2mk_BT - U/k_BT)$ is a solution of

$$
\frac{\partial \rho^{eq}}{\partial t} = \mathcal{L}^C \rho^{eq} = 0. \quad (12)
$$

If we turn on the drag force and the noise, we don't want the equilibrium distribution to move away from this distribution. This condition is satisfied only if $\mathcal{L}^D \rho^{eq} = 0$ also. This is precisely what Eq. (5) is designed for. If we do not choose the drag and noise weight functions according to Eq. (5), the simulation will move away from the equilibrium Gibbs-Boltzmann distribution when the drag and noise terms are turned on. In that case, although a steady state may be achieved, it may not be related to any recognized thermodynamic equilibrium distribution; there may not even be a recognizable Hamiltonian.

It is highly desirable to have a simulation in which the equilibrium distribution corresponds to the Gibbs-Boltzmann distribution. It means for instance that all the standard thermodynamic relations (for example, for the pressure) can be transferred to the new situation.

Now the reader may be wondering what is the point of dissipative particle dynamics, if all it achieves is to simulate a Hamiltonian system in the canonical ensemble. After all, this can be done by any one of a number of NVT molecular dynamics methods.[16] Indeed DPD can be viewed as a novel thermostatting method for molecular dynamics. Note though that DPD is an NVT method that *preserves hydrodynamics*. It has recently been suggested that the presence of hydrodynamics is important in annealing defects in ordered mesophases.[19] Thus DPD has an intrinsic advantage over other methods such as dynamic density functional theory (which are purely diffusive) or Monte Carlo methods, in trying to evolve a system towards an ordered thermodynamic equilibrium state.

As compared to usual molecular dynamics simulations, for example with Lennard-Jones atoms, the major advantage of the new method is its soft interaction potential $\mathbf{F}^C$. The particles represent molecules or liquid elements rather than atoms, and the soft potential allows for a much larger timestep than is commonly used in usual MD simulations. The question of the connection from atomistic parameters to mesoscopic parameters will be addressed in the remainder of this paper. Such soft interaction potentials could, of course, also be used in a standard MD type algorithm (given by the present algorithm with the noise and dissipative turned off: $\sigma = \gamma = 0$), or in a Monte Carlo algorithm.

Soft interactions have been proposed recently by Forrest and Suter.[20] Their approach is to start off bottom-up with atomistic (Lennard-Jones) interaction potentials, and to replace these by effective potentials between centres of mass. These effective potentials were obtained in a systematic way by averaging the molecular field over the rapidly fluctuating

motions of atoms during short time intervals. This approach leads to an effective potential similar to our Eq. (3). It does not diverge at $r=0$, and it no longer shows the characteristic minimum of the Lennard-Jones potential. This result supports our choice of a soft repulsive interaction force.

Although the approach of Forrest and Suter looks very promising, there are a number of comments to make. Firstly their procedure to obtain the effective ''time-averaged'' potentials involves complicated integrals, analogous to the calculation of virial coefficients in a low density expansion. Therefore, no explicit analytical expression can be obtained for the effective interaction potential. Furthermore, their numerical procedure neglects the correlation in the local density fluctuations, which involves the time-dependent pair correlation function. As such an approach becomes exceedingly complicated (though formally exact) we have chosen for a pragmatic alternative way to address the problem.

In the remainder of this paper we approach the connection between the atomistic potential and the mesoscopic interaction forces in a top-down approach, in which we start from the mesoscopic side. The strategy will be to match the thermodynamics of the DPD simulation to that of the underlying atomistic system.

First it is necessary to set length, time and mass scales for the simulation. The length and mass scales have already been set by specifying that particles have mass 1, and the cutoff distance for interactions is also 1 (obviously, these could be relaxed for mixtures). Rather than specify a unit of time, as Hoogerbrugge and Koelman do,[11] we choose to work in units such that $k_BT=1$, which effectively specifies a unit of time since the rms velocity of the particles is $\sqrt{3}$ from the Maxwell-Boltzmann distribution. Working in these units is useful since the conservative interaction potentials are automatically in units of k_BT without having to be rescaled.

III. HOW TO CHOOSE THE TIMESTEP AND NOISE LEVEL

The timestep size has to be chosen as a compromise between fast simulation and satisfying the equilibrium condition. We monitor this by monitoring the temperature of the system. Using Eq. (5) for a given noise amplitude and putting $k_BT=1$, the equilibrium temperature was measured from the velocities, as a function of the step-size

$$k_BT=\langle \mathbf{v}^2\rangle/3, \tag{13}$$

where $\langle \ldots \rangle$ is a simple average over all particles in the simulation.

Two types of noise have been used, uniformly distributed random numbers and Gaussian distributed random numbers of the same variance. Results obtained from simulations of a system containing 4000 particles in a cubic box of sizes $10\times10\times10$, repulsion parameter $a=25$ [see Eq. (3) for its definition], averaged over 200 time steps are shown in Fig. 1. Several versions were examined. For all data points the noise level was taken equal at $\sigma=3$. The error bars indicate the spread in the temperature.
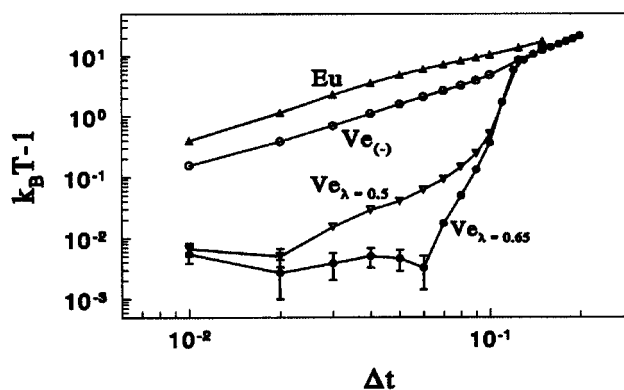

FIG. 1. Temperature as a function of timestep for $\sigma=3$, $\rho=4$. Curves are shown for the Euler-like algorithm Eq. (7) (Eu), the Verlet-like algorithm Eq. (9) (Ve) for two values of λ, and the Verlet-like algorithm without the acceleration term (Ve$_{(-)}$).

Several things are to be noted here. Firstly, no statistical difference was found between the simulations using uniform random numbers and the simulations using Gaussian random numbers. Since uniform random numbers take less CPU time to generate than Gaussian random numbers do, a choice for uniform noise is made. Secondly, the choice of the timestep is now determined by the amount of artificial temperature increase one is willing to accept. For the Verlet algorithm [$\lambda=1/2$ in Eq. (9)], with step size $\Delta t=0.04$ this increase is 2%, and at stepsize 0.05 it is 3%. Stepsize 0.04 thus seems a safe choice, and 0.05 an acceptable upper limit. To obtain the same degree of accuracy for the Euler algorithm would require timesteps of order $\Delta t\approx0.001$, i.e., the Verlet algorithm gives a factor of 50 or so improvement in performance.

Thirdly, it is also found that stable temperature control is obtained only when the term $\frac{1}{2}(\Delta t)^2\mathbf{f}(t)$ is included in the position update [see Eq. (9)]. If this term is left out, the results are nearly as bad as the Euler algorithm (see Fig. 1). Inclusion of this term in the Euler algorithm (not shown in Fig. 1) was found to improve temperature control to approximately the extent the Verlet algorithm without this term. Therefore inclusion of this term and the adoption of the Verlet algorithm are *both* essential to facilitate the use of a large timestep.

The reported temperature control holds for noise amplitude $\sigma=3$ and for $\lambda=0.5$ in Eq. (9). When the noise amplitude is reduced, the timestep range over which the system is stable does not change by much, but the speed at which the system reacts on temperature variations is reduced. For density $\rho=3$ and $\Delta t=0.04$ the system relaxes exponentially from temperature $k_BT=10$ to $k_BT=1$, where the relaxation time is some 10 timesteps. However, with noise amplitude $\sigma=1$ this relaxation time is some 90 timesteps, because the friction factor is a factor of 9 smaller in the latter case. If we study the temperature as a function of the noise amplitude, a plot similar to Fig. 1 is obtained: A slow increase of k_BT with σ is found up to $\sigma\approx8$ beyond which the temperature grows rapidly and the simulation may itself become unstable. Thus as a reasonable compromise between fast temperature equilibration, a fast simulation and a stable, physically meaningful system, simulation with stepsize $\Delta t=0.04$ and noise

amplitude $\sigma = 3$ is recommended with $\lambda = 0.5$ in the Verlet-type algorithm Eq. (9).

By empirically adjusting λ further gains are possible. For $\rho = 3$ and $\sigma = 3$, for example, we find the optimum value is $\lambda = 0.65$. For this value of λ we find that the timestep can be increased to $\Delta t = 0.06$ without significant loss of temperature control (see Fig. 1). The simulations in the remainder of this paper were all carried out with $\Delta t = 0.04$ and $\lambda = 0.5$ though.

IV. HOW TO CHOOSE THE REPULSION PARAMETER

Having established the parameters Δt and σ, which are related to the simulation method itself, we now turn to the parameters related to the simulated model. Inspecting Eq. (3), it is clear that there is only one parameter in this model, namely the repulsion parameter a. If the thermodynamic state of an arbitrary liquid is to be described correctly by the present soft sphere model, the fluctuations in the liquid should be described correctly. These are determined by the compressibility of the system, hence, analogously to the Weeks-Chandler-Anderson perturbation theory of liquids, we ought to choose our model such that

$$\kappa^{-1} = \frac{1}{nk_BT\kappa_T} = \frac{1}{k_BT}\left(\frac{\partial p}{\partial n}\right)_T \tag{14}$$

has the correct value. The parameter n appearing in Eq. (14) is the number density of molecules, and κ_T is the usual isothermal compressibility. For water at room temperature (300 K) this dimensionless compressibility has the numerical value $\kappa^{-1} = 15.9835$.

To find this correspondence, we have to establish the equation of state. Thus the pressure is obtained from simulation as a function of the density, for various repulsion parameters. Using the virial theorem, we obtain the pressure as

$$p = \rho k_BT + \frac{1}{3V}\left\langle \sum_{j>i}(\mathbf{r}_i - \mathbf{r}_j)\cdot\mathbf{f}_i \right\rangle$$

$$= \rho k_BT + \frac{1}{3V}\left\langle \sum_{j>i}(\mathbf{r}_i - \mathbf{r}_j)\cdot\mathbf{F}_{ij}^C \right\rangle$$

$$= \rho k_BT + \frac{2\pi}{3}\rho^2 \int_0^1 rf(r)g(r)r^2\,dr, \tag{15}$$

where $g(r)$ is the radial distribution function (see Fig. 2), and $\mathbf{f}_i$ and $\mathbf{F}_{ij}^C$ are the total and conserved parts of the force on particle i, respectively. In the simulation the second expression is used. Note that this expression is equal to the first only because our system has the correct Boltzmann distribution. If Eq. (5) is not satisfied, these two expressions are not equal in general.

As an explicit check, we have also used the first expression, and measured $g(r)$ and calculated the pressure afterwards using the third expression. This led to pressure differences of some 0.7%, i.e., negligible in practice. As a final check on programming errors, the pressure was also measured by introducing a soft wall in the system, and averaging the mean force exerted on the wall. Again good correspon-
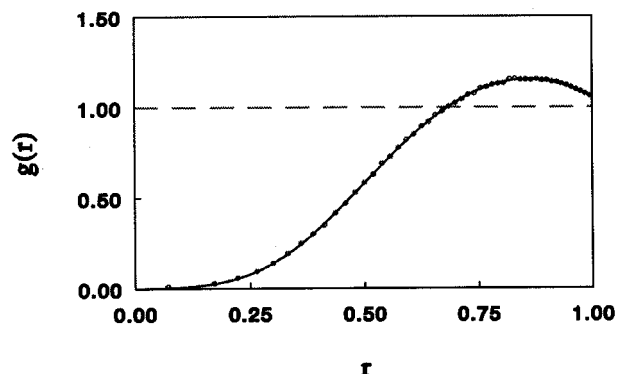

FIG. 2. Pair correlation function for the present soft sphere model, for $\rho = 3$ and $a = 25$.

dence was found: for two runs over 10^4 timesteps, for mean density $\rho = 5$, system size $8 \times 5 \times 5$ and repulsion $a = 15$, the pressure with noise included was 50.82 ± 0.05, without noise 50.59 ± 0.05 and the wall pressure was 50.92 ± 0.05. Hence, there is a small but finite difference between the two expressions for the virial pressure, but this difference does not occur if we look at the stress across an interface: If we study $p_{xx} - (p_{yy} + p_{zz})/2$, there is no systematic difference between the two methods. However, most importantly for measurements of surface tension (i.e., the integral over the stress across an interface), the error obtained when the noise is not included is a factor of 2.5 smaller than when the first expression from Eq. (15) is used.

To obtain the equation of state the density was varied from $\rho = 1$ to $\rho = 8$ in steps of 0.5 for repulsion $a = 15$, and less extensive density variations were studied for $a = 25$ and $a = 30$. After subtracting the ideal gas term it was found that the excess pressure scales linearly with the repulsion parameter. Furthermore, the excess pressure is dominated by a single ρ^2 term over a large range of densities. In Fig. 3 the results are shown for $a = 15$ (crosses), $a = 25$ (squares) and $a = 30$ (circles).

A somewhat more insightful picture emerges when we plot the excess pressure divided by ρ^2, which is shown in
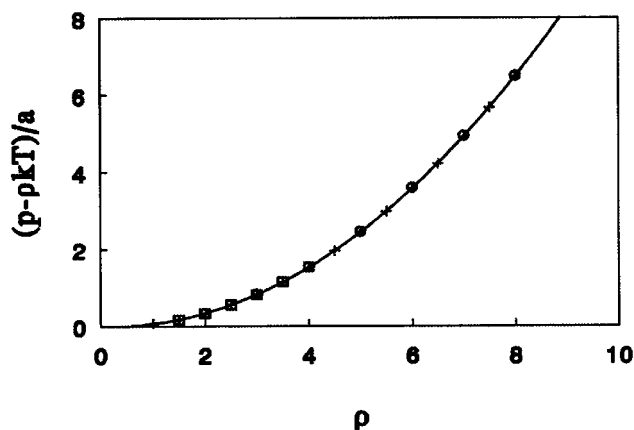

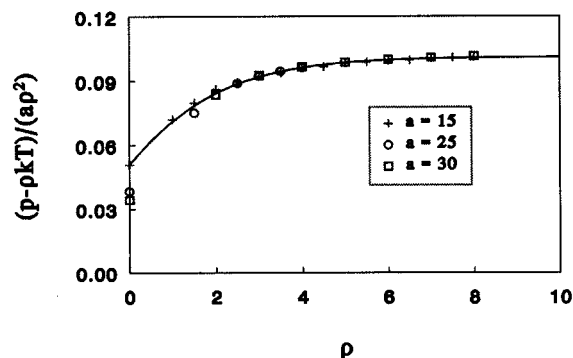FIG. 3. Excess pressure obtained from simulation. The full curve is a parabola fit.

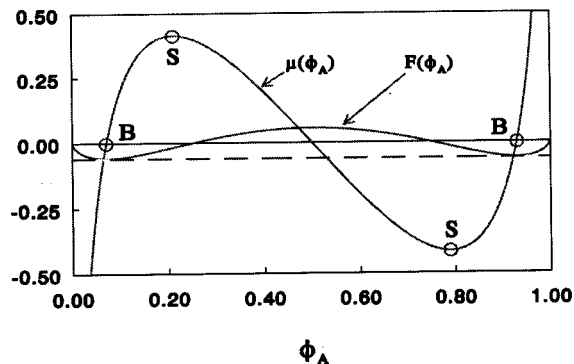FIG. 4. Excess pressure divided by $a\rho^2$ for three values of the repulsion parameter, showing scaling.

FIG. 5. Free energy and chemical potential in the Flory-Huggins model for $N_A = N_B = 1$. Points S are spinodal points; points B are binodal points of coexisting compositions.

Fig. 4. The points for $\rho = 0$ have been calculated from the virial expansion, Eq. (15) substituting the relation $g(r) = \exp(-\frac{1}{2}a(1-r)^2/k_B T)$. We find the virial coefficients 0.0509, 0.0384, and 0.0343 for $a = 15$, 25 and 30, respectively. What Fig. 4 now indicates is that for sufficiently large density, e.g., for $\rho > 2$, all systems fall on the same curve, indicating a simple scaling relation. Furthermore, since the curve in Fig. 4 levels off to a constant value by $\rho = 3$, the excess pressure is really proportional to ρ^2.

A good approximation for the pressure that holds for sufficiently high density ($\rho > 2$) is:

$$p = \rho k_B T + \alpha a \rho^2 (\alpha = 0.101 \pm 0.001). \tag{16}$$

This implies that the dimensionless compressibility, as introduced in Eq. (14), is given by $\kappa^{-1} = 1 + 2\alpha a\rho/k_B T \approx 1 + 0.2 a\rho/kT$. Combining this with the known compressibility of water, $\kappa_{\text{water}}^{-1} \approx 16$ we find $a\rho/k_B T \approx 75$. In principle the density chosen for the simulation is a free parameter, but since the number of interactions for each particle increases linearly with the density, the required CPU time per timestep and per unit of volume increases with the square of the density. For efficiency reasons one would thus choose the lowest possible density where the scaling relation still holds. From Fig. 4 it now follows that $\rho = 3$ is a reasonable choice; to have the compressibility of water, we need the repulsion parameter $a = 25 k_B T$. For other densities we use $a = 75 k_B T/\rho$.

V. MAPPING ONTO FLORY-HUGGINS

One objective to use the DPD method could be the simulation of liquids at interfaces. An obvious interface is the liquid-vapor interface, but here we have a problem. Since the repulsive pressure is so softly increasing with density, leading to the apparent absence of a ρ^3 term at high densities, the model cannot produce liquid-vapor coexistence. If the conservative force [Eq. (3)] is changed in such a way that the force is repulsive at small r, and attractive at large r, this attraction causes a reduction in the pressure proportional to ρ^2, which depends on temperature. This means that, when the temperature is chosen at a critical value, the pressure vanishes for a very broad range of densities as repulsive and attractive pressure exactly compensate. For temperatures

above this point the pressure is positive for all densities, and for temperatures below this point the system collapses. Hence, there is no real liquid vapor coexistence in this model. One may be tempted to change the repulsive force by introducing a steep repulsion at small r, but in doing so the temperature control is lost unless very small timesteps are taken. The whole advantage of the method is then lost.

While liquid-vapor interfaces cannot be simulated, one can simulate liquid-liquid and liquid-solid interfaces. In this way the method is similar to the Flory-Huggins theory of polymers, and can in fact be viewed as a continuous version of this lattice model. In the Flory-Huggins theory molecules of different length are confined to a lattice. The internal energy is described as a perturbation from ideal mixing, i.e., only the excess over pure components is taken into account. For two components this leads to the free energy per lattice site

$$\frac{F}{k_B T} = \frac{\phi_A}{N_A} \ln \phi_A + \frac{\phi_B}{N_B} \ln \phi_B + \chi \phi_A \phi_B, \tag{17}$$

where ϕ_A and ϕ_B are the volume fractions of the A and B components, N_A and N_B are the number of segments per A and B molecule, and the implicit condition is that the lattice is filled completely, hence $\phi_A + \phi_B = 1$. Under this condition $\phi_B = 1 - \phi_A$, and ϕ_A is the only degree of freedom.

When A and B are two components that do not favor contact the parameter χ is positive; when they favor each other over AA or BB contacts, then it is negative. For sufficiently large χ-parameters the free energy develops two minima, separated by a maximum, see Fig. 5. If $N_A = N_B$ the minimum free energy is found at $\mu = \partial F/\partial \phi_A = 0$. In Fig. 5 these points are indicated by a B. Their location follows from the implicit equation

$$\chi N_A = \frac{\ln[(1 - \phi_A)/\phi_A]}{1 - 2\phi_A}. \tag{18}$$

If χ is positive but too small, no segregation will take place, but when it exceeds a critical value A-rich and B-rich domains will occur. This critical χ-parameter is found from the condition that the spinodals (S in Fig. 5) coincide. This im-

plies that the first and second derivative of the chemical potential with respect to ϕ_A vanish, which leads to the critical point

$$\chi^{\text{crit}} = \frac{1}{2}\left(\frac{1}{\sqrt{N_A}} + \frac{1}{\sqrt{N_B}}\right)^2. \tag{19}$$

Since the present simulated system is fairly incompressible ($\kappa^{-1} = 16$), and since the excess pressure is quadratic in the density, the soft sphere model is by nature very close to the Flory-Huggins lattice model. The free energy density that corresponds to the pressure of a single component, Eq. (16), is

$$\frac{f_V}{k_B T} = \rho \ln \rho - \rho + \frac{\alpha a \rho^2}{k_B T}, \tag{20}$$

hence for a two component system of chains one expects

$$\frac{f_V}{k_B T} = \frac{\rho_A}{N_A}\ln \rho_A + \frac{\rho_B}{N_B}\ln \rho_B - \frac{\rho_A}{N_A} - \frac{\rho_B}{N_B}$$
$$+ \frac{\alpha(a_{AA}\rho_A^2 + 2a_{AB}\rho_A\rho_B + a_{BB}\rho_B^2)}{k_B T}. \tag{21}$$

If we choose $a_{AA} = a_{BB}$ and assume that $\rho_A + \rho_B$ is approximately constant,

$$\frac{f_V}{(\rho_A + \rho_B)k_B T} \approx \frac{x}{N_A}\ln x + \frac{(1-x)}{N_B}\ln(1-x) + \chi x(1-x)$$
$$+ \text{constants}, \tag{22}$$

where we have set $x = \rho_A/(\rho_A + \rho_B)$ and made the tentative identification

$$\chi = \frac{2\alpha(a_{AB} - a_{AA})(\rho_A + \rho_B)}{k_B T}. \tag{23}$$

Apparently we have the correspondence (soft spheres) $f_V/(\rho_A + \rho_B) = F$ (Flory-Huggins), with a χ-parameter mapping given by Eq. (23).

To test this relation simulations have been performed for binary mixtures of both monomers and polymers, at $\rho = \rho_A + \rho_B = 3$ and $\rho = 5$, for repulsion parameters $a = a_{AA} = a_{BB} = 25$ and $a = 15$, respectively. When the excess pressure was measured as a function of the fraction x of A particles it was found that it is indeed proportional to $x(1-x)$. However, unlike the assumption in Eq. (22) it was found that the prefactor of $x(1-x)$ is not simply linear in $\Delta a = a_{AB} - a$ when Δa is 2 to 5. In practice we are not interested in small differences in the repulsion, but systems will rather be chosen where segregation takes place, i.e., $\chi > \chi^{\text{crit}}$. Now if χ is much larger than the critical value, mean field theory is expected to be valid. This means that we can use Eq. (18) as the defining equation for the corresponding Flory-Huggins parameter.

Adopting this strategy, a system of size $8 \times 8 \times 20$ containing 3840 monomers was simulated. Half the particles were of type A and in the initial configuration they were placed in the left half of the system, the other particles, of type B, were placed in the right hand side. For these systems
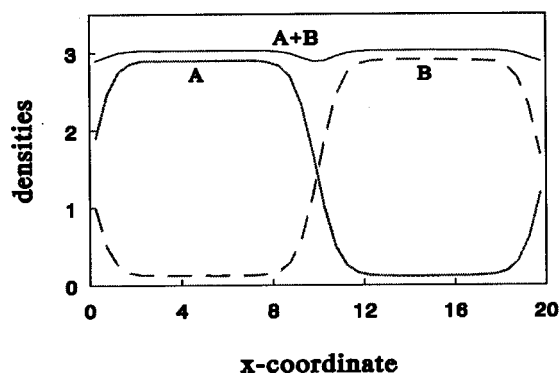

FIG. 6. Density profile for $\rho = 3$ at repulsion parameters $a_{AA} = a_{BB} = 25$ and $a_{AB} = 37$.

the density profiles of A and B particles were sampled across the interface. Averages of the density were taken over 10^5 timesteps; the mean value of x over a slab where the density is homogeneous was then taken to compute the corresponding Flory-Huggins parameter. An example of such a binary density profile is shown in Fig. 6. Note the small dip in the sum of the densities at the interface.

When the measured segregation parameter x is substituted for ϕ_A in Eq. (18), the Flory-Huggins parameter for monomers is found. Now, when we are close to the critical point ($\chi = 2$), we cannot expect this mean-field expression to hold, but when we calculate for $\chi > 3$ this value should be reliable. The calculated χ-parameter is shown in Fig. 7 for two densities as a function of the excess repulsion parameter. We find that for $\chi > 3$ there is a very good linear relation between χ and Δa. Explicitly, we have

$$\chi = (0.286 \pm 0.002)\Delta a (\rho = 3),$$
$$\chi = (0.689 \pm 0.002)\Delta a (\rho = 5). \tag{24}$$

These results partly confirm Eq. (23) in that χ is linear in Δa, but the constant of proportionality is far from linear in the density. Nevertheless, we can choose a fixed density, and henceforth use Eqs. (24) as an effective mapping on the Flory-Huggins theory.
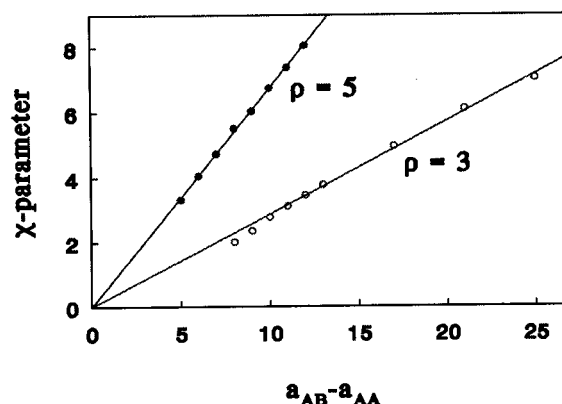

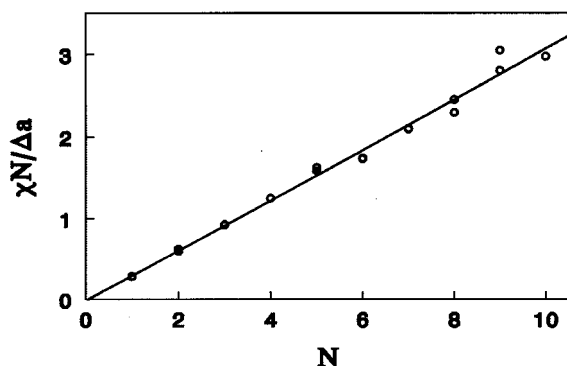FIG. 7. Relation between excess repulsion and effective χ-parameter.

FIG. 8. Simulation results for the effective χ-parameter as a function of polymer length.

Polymer systems were studied next. To make a polymer, monomers are threaded together in linear chains, using the interaction force

$$\mathbf{f}_i^{(\text{spring})} = \sum_j C\mathbf{r}_{ij}, \tag{25}$$

where the sum runs over all particles to which particle i is connected. The spring constant is chosen such that the mean distance between connected particles coincides with the point where the pair correlation function has its maximum, see Fig. 2. For $\rho = 3$ and $a = 25$, this occurs for $C \approx 2$. If we choose C much larger, the particles are tied together at very short distance and we get very stiff chains, and if we take it much smaller we get a longer distance between the connected particles than between unconnected nearest neighbors. Hence $C = 2$ seems a reasonable choice. This spring force is similar to the "weak spring" of Schlijper et al.[14]

Between particles of the same type the repulsion parameters are taken as $a_{ii} = 75k_BT/\rho$ for all types, and the cross terms are again chosen as

$$a_{ij} = 75k_BT/\rho + \Delta a \quad (i \neq j) \tag{26}$$

which defines the excess repulsion Δa. The polymer length, $N = N_A = N_B$ was varied from 2 to 20, and the repulsion parameter was varied from $\Delta a = 1$ to 40.

The Flory-Huggins χ-parameter for polymers was obtained via the observed segregation. The result for $\chi N/\Delta a$ is plotted as a function of N in Fig. 8. We find that the $N = 1$ results all lie systematically below the line of the $N > 1$ results, but the difference is only some 7%. The best estimate obtained for $2 < N < 10$ is

$$\frac{\chi N k_B T}{\Delta a} = (0.306 \pm 0.003)N. \tag{27}$$

A possible off-set at $N = 0$ has been investigated. Including the $N = 1$ results the off-set defined in the equation $\chi N k_B T/\Delta a \propto (N - N_0)$ is $N_0 = 0.038 \pm 0.11$, and if we neglect the $N = 1$ results the off-set $N_0 = -0.002 \pm 0.2$ is found. Hence in either case the off-set is zero well within the accuracy of the fit.

VI. SURFACE TENSION BETWEEN HOMOPOLYMER MELTS

The surface tension between unlike polymers of equal length is also determined in the simulations above. This is a case where few results are available, thus it also illustrates the application of the method to a real polymer problem. A very useful scaling relation is found, which facilitates the extrapolation of simulations on small polymers to the real world of very long polymers.

For very long chains the ln terms in Eq. (17) drop out, leading to a free energy $F/k_BT = \chi\phi_A\phi_B$. In this case the surface tension becomes independent of the polymer length, for which case Helfand has derived the analytic expression[21]

$$\sigma = \tfrac{1}{2}k_BT(\chi m)^{1/2}[1 + (1 + \chi)\chi^{-1/2}\tan^{-1}\chi^{1/2}], \tag{28}$$

where m is the fraction of contacts a lattice site has perpendicular to the interface, relative to the total number of contacts it has. This equation has two limiting results. In general, the surface tension equals χ times the width of the interface. At small χ the width is proportional to $\chi^{-1/2}$, and hence the surface tension is proportional to $\chi^{1/2}$. As χ increases, the interface narrows, and at a certain stage it has the width of a single lattice cell. Beyond that point the interface cannot narrow down any further, hence the surface tension must become simply proportional to χ. In this limit the specific lattice nature of the approximation becomes apparent. In the small χ limit, where the width of the interface is much larger than a lattice spacing, the result should not be affected by the lattice approximation, the surface tension on a simple cubic lattice is $\sigma = k_BT(\chi/6)^{1/2}$.

The surface tension for finite polymer length has been derived only as an asymptotic expansion in N in the form

$$\sigma = k_BT\left(\frac{\chi}{6}\right)^{1/2}\left(1 - \frac{k}{\chi N} + O\left(\frac{1}{(\chi N)^2}\right)\right). \tag{29}$$

Broseta et al.[22] find $k = \pi^2/6$ whereas Helfand et al.[23] find $k = 2\ln 2$. The prefactor $(\chi/6)^{1/2}$ is Helfand's earlier $N = \infty$ result, and the difference in the prefactor of $1/\chi N$ is caused by slight differences in the approximation used.

At this point it should be noted that for simple liquids, the surface tension near the critical point behaves as[24]

$$\sigma \sim (1 - T/T_c)^\mu, \tag{30}$$

where the exponent $\mu = 3/2$ in classical van der Waals theory, whereas the renormalization theory result for the critical exponent is $\mu = 1.26$ for the Ising model. Since the χ-parameter is a Gibbs free energy divided by k_BT, we can make the identification $T \to 1/\chi N$. It can thus be expected that we can use Eq. (30) with this substitution to replace the $1/\chi N$ expansion given above, and obtain an expression that is valid up to the critical point.

To measure the surface tension in the present simulations, the difference between the normal and tangential stress was integrated across the interface

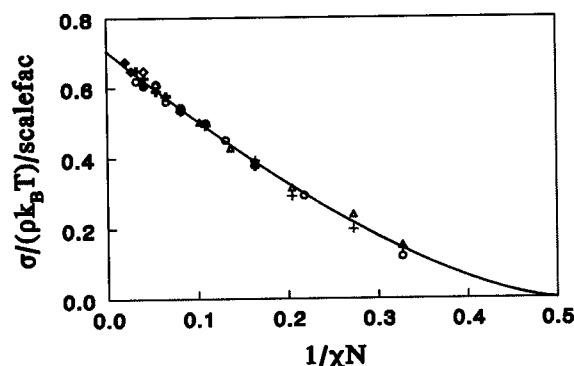$$\sigma = \int [p_{zz}(z) - \tfrac{1}{2}(p_{xx}(z) + p_{yy}(z))]dz. \tag{31}$$

FIG. 9. Re-scaled surface tension as a function of $1/\chi N$. For each data set N is varied and χ is kept fixed. The smooth curve is a fit to a 3/2 power law.

FIG. 10. Scale factors used in Figure 9 as a function of χ. The straight line fit has slope 0.403 ± 0.009.

The components of the stress tensor were obtained from the tensor equivalent of the second line of Eq. (15).

First we study the surface tension for the case $N > 1$. In general we can expect that the surface tension is given by some scaling function of χN, i.e.,

$$\sigma \sim \chi^{\alpha} g(\chi N). \tag{32}$$

As in Flory-Huggins theory of polymers it has been found that for large arguments the scaling function $g(x)$ is linear in $1/x$, we plot the simulated surface tension against $1/\chi N$ in Fig. 9. For each data set the polymer length N was varied, while Δa (and hence χ) was kept fixed. To eliminate the χ-dependent pre-factor in Eq. (32) all surface tensions were rescaled so that they would best fit the surface tension at $\Delta a = 5$ (i.e., $\chi = 1.53$). The functional relation in Fig. 9 is therefore $g(x)$.

It is now a fitting exercise to obtain an explicit functional form. A three parameter fit of the form $g(\chi N) = k(1 - \chi^{\text{crit}}/\chi N)^{\mu}$ gives $\chi^{\text{crit}} = 1.94 \pm 0.14$ and $\mu = 1.62 \pm 0.17$, i.e., within the error we find the mean-field critical point and the classical Van der Waals exponent. If we force $\chi^{\text{crit}} = 2$, we find from a two parameter fit $\mu = 1.55 \pm 0.03$, confirming the classical value of the exponent.

To obtain the χ-dependent prefactor in Eq. (32) the scaling factors used to rescale all data to the same master curve in Fig. 9, are plotted as a function of χ in Fig. 10. All points fall on a straight line of slope 0.403 ± 0.009 confirming the power law assumption in Eq. (32). However, the value of this exponent is lower than expected, as mean-field Flory-Huggins theory predicts $\alpha = 1/2$. The scaling law obtained from the present simulations thus takes the form

$$\sigma = (0.583 \pm 0.004) \rho k_B T r_c \chi^{0.4} [1 - 2/(\chi N)]^{3/2} \tag{33}$$

which is shown in Fig. 11.

The scaling curve shown in Fig. 11 has been compared to experimental data on PS/PMMA surface tension.[25] The data were read off Fig. 6 of this reference; the molecular mass varies from $M_n = 1700$ up to $M_n = 43500$. Since the combination of surface tension in Fig. 11 has the dimension length (the DPD interact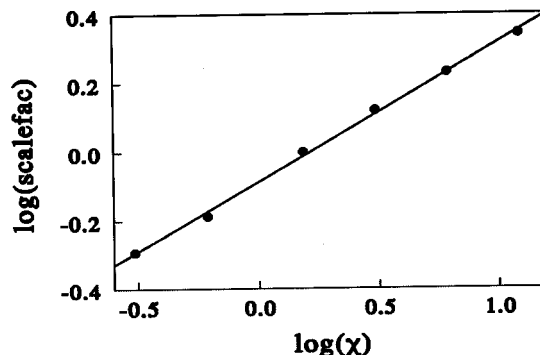ion radius) which is not known at forehand, and since χ-parameter and Kuhn length for this system are unclear, the experimental data were rescaled in both x and y directions to match our universal curve. The experimental points are shown with error bars. Naturally, in this particular example only the shape of the curve is compared with the simulation results, rather than absolute values, but it does illustrate that the DPD simulation results can be used for quantitative predictions on real systems. By combining similar experiments and the present scaling curve, a quantitative mapping of long polymers on relatively small DPD chains can thus be made.

Now we turn to the case $N = 1$. If we use the function in Eq. (33) to fit the surface tension, we find a prefactor 0.495 ± 0.006. The difference with the numerical factor in Eq. (33) is clearly outside the estimated range of uncertainty, hence the $N = 1$ case does not conform to this scaling law. Furthermore, we find the surface tension clearly to extrapolate to a higher critical point than $\chi^{\text{crit}} = 2$, see Fig. 12. This implies that the $N = 1$ system behaves non-classically. A three parameter fit of the form $\sigma = k\chi^{\alpha}(1 - \chi^{\text{crit}}/\chi)^{1.5}$ gives $\alpha = 0.26 \pm 0.01$ and $\chi^{\text{crit}} = 2.36 \pm 0.02$. This confirms the non-classical value of the critical point. For consistency this would imply that the Ising exponent $\mu = 1.26$ should be pertinent, which leads to $\alpha = 0.31 \pm 0.01$ and $\chi^{\text{crit}} = 2.49 \pm 0.02$.
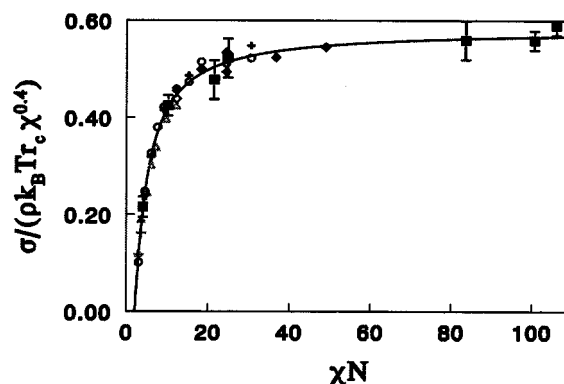

FIG. 11. Simulated polymer surface tension master curve. The points with error bars are experiments on PS/PMMA interfaces (Ref. 25).
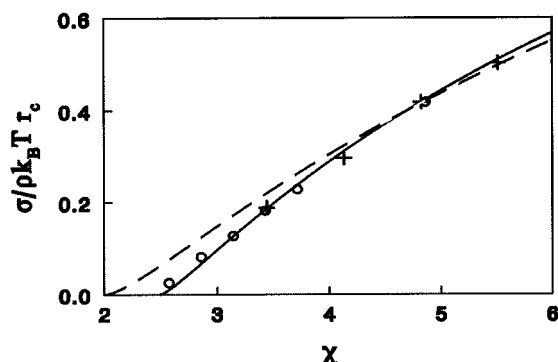
FIG. 12. Single bead surface tension. The dashed curve is a fit based on the mean field critical point and exponents, the full curve is a fit based on mean field exponents and a non-classical critical point.
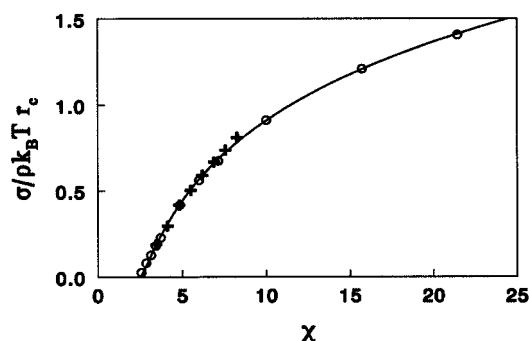

FIG. 13. Surface tension of single DPD beads, the fit is based on classical exponents with a non-classical critical point [Eq. (36) in the text]. Crosses: $\rho = 5$; circles: $\rho = 3$.

Although the fit with $\mu = 1.5$ is slightly better than the fit with $\mu = 1.26$, the difference is so small that we cannot distinguish between the two on the basis of this data.

To further investigate the nature of the exponent for $N = 1$, we also studied the width of the interface. The density profile was fitted to the functional form

$$\rho(z) = \tfrac{1}{2}\rho_0[\tanh(2(z-z_0)/\xi)+1], \tag{34}$$

where ρ_0, z_0 and ξ were free fit parameters, and ξ is a measure of the width of the interface. In general the correlation length should diverge as $\xi \sim (\chi - \chi^{\text{crit}})^{-\nu}$, where $\nu = 1/2$ if the classical set of critical exponents is pertinent, and $\nu = 0.63$ for the Ising model. Both for the $\rho = 3$ and for the $\rho = 5$ data the width of the interface close to the critical point is well described by

$$\xi = \frac{3.24 \pm 0.03}{\sqrt{\rho(\chi - (2.39 \pm 0.03))}} \tag{35}$$

which is found by plotting ξ^{-2} against χ. When we plot $\xi^{-1.6}$ against χ (assuming $\nu = 0.63$) we find a line that extrapolates to zero by $\chi^{\text{crit}} = 2.10 \pm 0.04$. This value is not consistent with the critical point found from the surface tension, when non-classical exponents were assumed. The critical point found from surface tension and from the width of the interface are consistent with each other only when we assume classical exponents. Therefore, we conclude that, although the value of the critical point is non-classical, the behavior of the $N = 1$ system is still governed by classical exponents, even quite close to the critical point. Our best fit of the surface tension is

$$\sigma = (0.75 \pm 0.02)\rho k_{\text{B}} T r_c \chi^{0.26 \pm 0.01}$$
$$\times [1 - (2.36 \pm 0.02)/\chi]^{3/2}. \tag{36}$$

It should be remarked that Fig. 13 contains data obtained from $\rho = 3$ and from $\rho = 5$, where χ was calculated from $\chi = 0.286\Delta a$ for $\rho = 3$, and from $\chi = 0.689\Delta a$ for $\rho = 5$ [see Eq. (24)].

VII. DYNAMICS

The previous sections were essentially concerned with the equilibrium behavior of DPD. Here we discuss more briefly the dynamics of a DPD fluid, in particular with respect to polymer solutions. Apparently successful simulations have been reported in the literature,[14] but here we indicate a possible problem concerning the separation of the timescale for the propagation of hydrodynamic interactions and the timescale for diffusion. More detailed investigations of the dynamics of a DPD fluid are being currently undertaken. A quantity of key interest in this respect is the Schmidt number $\text{Sc} = \nu/D$, where ν is the kinematic viscosity and D is the diffusion constant. It is a dimensionless parameter characterizing the fluid, and can be interpreted as the ratio between the time for fluid particles to diffuse a given distance, to the time for hydrodynamic interactions to reach steady state on the same distance. Equivalently it measures the ratio of particle diffusion to momentum diffusion. In a typical fluid, water for instance, Sc is of order 10^3, reflecting the fact that momentum is transported more efficiently than particles, as a consequence of the caging effect of the interparticle potential. Since in DPD, very soft potentials are used, this caging effect is expected to be reduced, and one might expect Sc to be reduced. A simple calculation given below indicate that this is indeed the case.

The transport properties of the DPD fluid have been investigated by several workers.[11,26] Simplified arguments leading to these results are presented in the Appendix. For the self-diffusion coefficient of a DPD particle we find $D \approx 45 k_{\text{B}} T/2\pi\gamma\rho r_c^3$. For the kinematic viscosity we find $\nu \approx D/2 + 2\pi\gamma\rho r_c^5/1575$, where the first term is a kinetic contribution and the second comes from the dissipative forces. Contributions from the conservative forces have been neglected. The Schmidt number follows from these as

$$\text{Sc} \approx \frac{1}{2} + \frac{(2\pi\gamma\rho r_c^4)^2}{70875 k_{\text{B}} T}. \tag{37}$$

We have tested the accuracy of these estimates by simulations on single system only, with $\gamma = 6.75$ and $\rho = 3$. From the simulations we find $D = 0.306 \pm 0.006$, $\nu = 0.305 \pm 0.005$ and hence $\text{Sc} = 1.00 \pm 0.03$.[27] Inserting the appropriate pa-

rameters in the approximate theoretical expressions give $D = 0.354$, $\nu = 0.258$ and $Sc = 0.728$ which are within ~ 10–30% of the measured results. The important point is that the Schmidt number is about three orders of magnitude lower than that of a real fluid.

Such a small value implies that particles are diffusing as fast as momentum in the fluid. Contrast this with the Zimm model for polymer dynamics for instance where, in order to calculate the effect of hydrodynamic interactions, the Oseen tensor is used.[28] The use of the Oseen tensor amounts to the assumption that hydrodynamic interactions have reached a steady state on the timescale of polymer motion. This is entirely reasonable when the Schmidt number is large as it is in a real fluid, but is not clearly the case for DPD as discussed here. The result for DPD would be that hydrodynamic interactions are still developing on the timescale that the polymer beads are diffusing, i.e., the dynamics of the polymer and the fluid velocity field have become coupled. What the actual effect on the dynamics of a polymer in solution is at present unclear.

It might be remarked that the relaxation of a polymer chain is slowed down compared to the diffusion of isolated monomers. This is true, but it does not improve the situation greatly. The slowest relaxation mode of a polymer chain is associated with diffusion of its center of mass. If D is taken to be the diffusion constant associated with this mode, then the Schmidt number is increased roughly by a factor R_H, where R_H is the hydrodynamic radius of the chain (this is because $D_{polymer} \approx D_{monomer}/R_H$). Since chain lengths are likely to be of order 10–100 monomers in a practical simulation, this enhancement factor may only be of order 5–10 or so.

The same remarks also apply to the simulation of colloidal particles. The value of ν/D for a colloidal particle (where D is now the diffusion constant of the colloidal particle) is often of order 10^6 in a real suspension. Similar to polymers, one may anticipate $D \propto 1/a$ for large particles of radius a in a fluid of smaller particles. For a simulation where the colloid particle radius is $a \approx 5 r_c$ or so, $\nu/D \lesssim 10$ is expected. Again it is not exactly transparent what the effect of such as low value for ν/D has on the behavior of a simulated colloidal suspension, although it has been demonstrated by lattice Boltzmann simulations that $\nu/D \gtrsim 750$ is required in order that the short time diffusion in a colloidal suspension asymptote to the correct value.[29] Ladd has noted that lattice gases suffer from the same defect.[30]

Equation (37) suggests a possible solution to this problem since it indicates that Sc increases linearly with γ^2. That Sc should increase with γ might be expected intuitively since an increase in the dissipation should lead both to a slowed diffusion and to an increased viscosity. Thus higher values of the Schmidt number may be attainable by using larger values of γ than we have used in the main part of this paper. At the same time though, Δt would have to be reduced to maintain the temperature control. Whether large enough Schmidt numbers can be achieved in a practical simulation for a system to be in the correct regime of dynamic behavior is currently under investigation.

VIII. CONCLUSIONS

In this paper the DPD method is critically reviewed. It is described in detail how the noise amplitude, friction factor and timestep may be chosen. The method can be viewed upon as a molecular dynamics method with added noise, similar to Brownian dynamics or Langevin dynamics. The model used to describe the liquid consists of very soft, repulsive spheres; this is the reason why large timesteps can be taken.

To describe the density fluctuations as they appear in a molecular liquid correctly, the compressibility in the simulation model is matched to the compressibility of the liquid to be studied. From this condition the repulsion parameters between equal particles can be fixed. In the present model it is not possible to have liquid-vapor coexistence; in this aspect the method is similar to the Flory-Huggins theory of polymers, and to regular solution theory. In these widely used theories, molecular interactions between unequal segments on a lattice are characterized by χ-parameters. In the present work a relation between these χ-parameters and the repulsion parameters between unequal particles in the simulation has been derived, by applying the condition that the solubility of one phase into the other should be described correctly. The model described can be viewed as an off-lattice simulation method for Flory-Huggins models.

This work therefore opens the way to do large scale simulations, effectively describing millions of atoms, by using a two-stage approach. First, mutual solubility and compressibility of liquids consisting of parts of (macro)molecules can be calculated using simulations retaining all atomistic details. Then these simulation results can be fed into a mesoscopic DPD simulation to study the formation of micelles, networks, mesophases and so forth. This effectively bridges the gap between the atomistic length scale and the mesoscopic length scale. It puts us in the position to predict the mesoscopic structure of surfactants and long polymers, with arbitrary branching and loop structure, using a direct simulation method.

For instance, the micro-phase separation properties of polymers of length $N = 10^4$ can be represented by the simulation of polymers of length $N = 10$, if at the same time the χ-parameter is increased by a factor 10^3 (assuming the original χ-parameter was small). Thus the driving force for (micro)-phase separation, the surface tension, increases with a factor of 16. Furthermore the typical time for rearrangements in the polymer structure, the Zimm time which is proportional to $N^{3/2}$, is reduced by a factor $10^{9/2} \approx 3 \times 10^4$. Combining these factors show that we gain a factor of 5×10^5 in simulation speed to arrive at the equilibrium state in this example.

As an example of this, a scaling relation for the surface tension between two phases of equal length polymers has been derived from DPD simulations, and presented in terms of the Flory-Huggins χ-parameter. A difference is found between single DPD particles and DPD polymers. For single particles the critical χ is larger than predicted from mean-field theory, but for polymers the mean-field prediction for

the critical point is correct within the simulation error. Also, for polymers the mean-field value for the surface tension critical exponent ($\mu = 3/2$) is recovered within the simulation error. For single particles the value of this exponent is less certain, but combination with the divergence of the width of the interface (the correlation length) shows that the behavior is still governed by classical exponents ($\nu = 1/2$, $\mu = 3/2$) even quite close to the non-classical critical point.

We have also discussed dynamics briefly, which is a topic currently under investigation. We have indicated a possible problem with DPD in that the rate of particle transport due to diffusion is of the same order of magnitude as momentum transport. Practically, this means that the particles in a polymer chain are liable to be changing position on the same timescale as hydrodynamic interactions develop between them. This is in contrast to what is expected in a real fluid. However, it should not affect the equilibrium behavior. Indeed the presence of ''soft'' hydrodynamic deformation modes allows the polymers to reach equilibrium more easily than they would if they were to rely on pure diffusion.

ACKNOWLEDGMENTS

APPENDIX; APPROXIMATE EXPRESSIONS FOR TRANSPORT COEFFICIENTS

In this Appendix we present simplified derivations for viscosity and self-diffusion coefficient in which the physical origin is hopefully transparent. Firstly, the viscosity of a DPD fluid has been derived independently by several workers.[12,26] Consider a fluid undergoing uniform linear flow $v_\alpha = e_{\alpha\beta} r_\beta$. (In this section Greek indices indicate spatial components, and summation convention is used.) The idea is that the dissipative contribution to the stress is due to the explicit friction force acting between particles moving on different streamlines. The kinetic contribution is due to particles (i.e., momentum carriers) diffusing across streamlines and is related to the particle self diffusion coefficient. It will be dealt with later. First though, the dissipative contribution is [compare Eq. (15)]

$$\sigma_{\alpha\beta} = \frac{1}{V} \left\langle \sum_{i>j} r_{ij\alpha} F^D_{ij\beta} \right\rangle. \tag{A1}$$

The drag force is given in Eq. (4) and is

$$\mathbf{F}^D_{ij\beta} = \gamma w^D(r_{ij}) \hat{r}_{ij\beta} \hat{r}_{ij\gamma} v_{ij\gamma} = \gamma w^D(r_{ij}) \hat{r}_{ij\beta} \hat{r}_{ij\gamma} e_{\gamma\delta} r_{ij\delta}. \tag{A2}$$

In the second line the velocity of the ith particle is taken to be that of the fluid at the same position. Inserting this in the previous expression, replacing the sum over i and j with an integral, and assuming a uniform density ($g(r) = 1$), one obtains

$$\sigma_{\alpha\beta} = \frac{\rho^2}{2} \int d^3\mathbf{r} \, \gamma w^D(r) r_\alpha \hat{r}_\beta \hat{r}_\gamma r_\delta \, e_{\gamma\delta}$$
$$= \frac{2\pi\gamma\rho^2}{15} \int_0^\infty dr \, r^4 w^D(r) [e_{\alpha\beta} + e_{\beta\alpha} + \delta_{\alpha\beta} e_{\gamma\gamma}]. \tag{A3}$$

This allows identification of the dissipative contribution to viscosity

$$\eta^D = \frac{2\pi\gamma\rho^2}{15} \int_0^\infty dr \, r^4 w^D(r) \tag{A4}$$

and second viscosity $\zeta^D = 5\eta^D/3$. These results are in agreement with those derived by a more sophisticated technique.[26] Inserting the expression for the dissipative function gives the dissipative contribution to the viscosity used in the main text: $\nu^D = \eta^D/\rho = 2\pi\gamma\rho r_c^5/1575$.

We now turn to a derivation for the self diffusion coefficient. Focus on the equation of motion of a single particle and ignore the conservative forces

$$\frac{d\mathbf{v}_i}{dt} = \sum_{j \neq i} \mathbf{F}^D_{ij} + \sum_{j \neq i} \mathbf{F}^R_{ij}. \tag{A5}$$

The drag force is linear in the velocity difference and thus the part due to the motion of the ith particle may be separated out. Dropping the other part but retaining the random force gives a Langevin equation for the motion of the ith particle

$$\frac{d\mathbf{v}_i}{dt} + \frac{\mathbf{v}_i}{\tau} = \mathbf{F}^R, \tag{A6}$$

where

$$\frac{1}{\tau} = \sum_{j \neq i} \gamma w^D(r_{ij}) \frac{\hat{\mathbf{r}}_{ij} \cdot \hat{\mathbf{r}}_{ij}}{3}, \quad \mathbf{F}^R = \sum_{j \neq i} \sigma w^R(r_{ij}) \theta_{ij} \hat{\mathbf{r}}_{ij}. \tag{A7}$$

Replacing the sum for the drag factor by an integral, and likewise in the calculation of the statistics of the random force $\mathbf{F}^R$, obtains

$$\frac{1}{\tau} = \frac{4\pi\gamma\rho}{3} \int_0^\infty dr \, r^2 w^D(r),$$

$$\langle \mathbf{F}^R \rangle = 0, \quad \langle \mathbf{F}^R(t) \cdot \mathbf{F}^R(t') \rangle$$
$$= 4\pi\sigma^2\rho \int_0^\infty dr \, r^2 [w^R(r)]^2 \delta(t - t'). \tag{A8}$$

The Langevin equation is solved straightforwardly to obtain $\langle \mathbf{v}_i(0) \cdot \mathbf{v}_i(t) \rangle = 3k_B T e^{-t/\tau}$ and therefore

$$D = \frac{1}{3} \int_0^\infty dt \langle \mathbf{v}_i(0) \cdot \mathbf{v}_i(t) \rangle = \tau k_B T. \tag{A9}$$

The fluctuation-dissipation theorem in this case takes the form

$$\sigma^2 \int_0^\infty dr\, r^2 [w^R(r)]^2 = 2\gamma k_B T \int_0^\infty dr\, r^2 w^D(r), \qquad \text{(A10)}$$

thus the temperature appearing in this analysis is the same as that in the true fluctuation-dissipation theorem Eq. (5) despite the approximations made. Inserting the expression for the dissipative function gives the self-diffusion coefficient used in the main text: $D = 45 k_B T / 2\pi \gamma \rho r_c^3$. This result for the self-diffusion coefficient is in agreement with that derived by more sophisticated means.[26]

Finally, the kinetic contribution to stress may now be estimated. From simple kinetic theory[31] the viscosity is $\eta^K = \rho \langle \mathbf{v}^2 \rangle \tau / 3$, where τ is the mean time between collisions. Since $\langle \mathbf{v}^2 \rangle = 3 k_B T$, and the velocity autocorrelation function derived above suggests a natural timescale, we expect $\nu^K \propto \tau k_B T = D$. Here, the more sophisticated calculation[26] gives a numerical prefactor and shows that $\nu^K = D/2$. The kinetic and dissipative contributions are simply added.

[1] R. D. Groot and W. G. M. Agterof, J. Chem. Phys. **100**, 1649, 1657 (1994).

[2] R. D. Groot and W. G. M. Agterof, Macromolecules **28**, 6284 (1995).

[3] R. D. Groot, A. Bot, and W. G. M. Agterof, J. Chem. Phys. **104**, 9202 (1996).

[4] P. G. de Gennes and C. Taupin, J. Phys. Chem. **86**, 2294 (1982).

[5] T. Odijk, Langmuir **8**, 1690 (1992).

[6] D. J. Mitchell, G. J. T. Tiddy, L. Waring, T. Bostock, and M. P. McDonald, J. Chem. Soc., Faraday Trans. 1 **79**, 975 (1983).

[7] F. S. Bates and G. H. Frederickson, Annu. Rev. Phys. Chem. **41**, 525 (1990).

[8] R. G. Larson, J. Chem. Phys. **91**, 2479 (1989).

[9] L. Leibler, Macromolecules **13**, 1602 (1980); M. W. Matsen and M. Schick, Phys. Rev. Lett. **72**, 2660 (1994).

[10] J. G. E. M. Fraaije, J. Chem. Phys. **99**, 9202 (1993).

[11] P. J. Hoogerbrugge and J. M. V. A. Koelman, Europhys. Lett. **19**, 155 (1992).

[12] J. M. V. A. Koelman and P. J. Hoogerbrugge, Europhys. Lett. **21**, 363 (1993).

[13] Y. Kong, C. W. Manke, W. G. Madden, and A. G. Schlijper, Int. J. Thermophys. **15**, 1093 (1994).

[14] A. G. Schlijper, P. J. Hoogerbrugge, and C. W. Manke, J. Rheol. **39**, 567 (1995).

[15] P. Español and P. B. Warren, Europhys. Lett. **30**, 191 (1995).

[16] M. P. Allen and D. J. Tildesley, *Computer Simulation of Liquids* (Clarendon, Oxford, 1987).

[17] H. C. Öttinger, *Stochastic Processes in Polymeric Fluids* (Springer, New York, 1996). This book contains recipes for higher order schemes which could be applied to DPD. The largely heuristic algorithm in Eq. (9) does not appear to map easily on to these though. It is possible that one of these more sophisticated algorithms could further improve the efficiency of the simulation.

[18] As noted by Español and Warren (Ref. 15), there is no difficulty of interpretation of the stochastic differential equations—the Itô and Stratonovich interpretations coincide. This also means that there are no diffusion tensor gradient terms in the first order Euler scheme.

[19] G. Gonella, E. Orlandini, and J. M. Yeomans, Phys. Rev. Lett. **78**, 1695 (1997).

[20] B. M. Forrest and U. W. Suter, J. Chem. Phys. **102**, 7256 (1995).

[21] E. Helfand, J. Chem. Phys. **63**, 2192 (1975).

[22] D. Broseta, G. H. Frederickson, E. Helfand, and L. Leibler, Macromolecules **23**, 132 (1990).

[23] E. Helfand, S. M. Bhattacharjee, and G. H. Frederickson, J. Chem. Phys. **91**, 7200 (1989).

[24] J. S. Rowlinson and B. Widom, *Molecular Theory of Capillarity* (Clarendon, Oxford, 1982).

[25] S. H. Anastasiadis, I. Gancarz, and J. T. Koberstein, Macromolecules **21**, 2980 (1988).

[26] C. Marsh, G. Backx, and M. H. Ernst, Europhys. Lett. **38**, 411 (1997).

[27] The observation that $\nu = D$ within the errors is a coincidence dependent on the particular simulation parameters; ν and D move in different directions as γ is varied.

[28] M. Doi and S. F. Edwards, *Theory of Polymer Dynamics* (Clarendon, Oxford, 1990).

[29] O. P. Behrend, Ph.D. thesis, University of Edinburgh, 1994.

[30] A. J. C. Ladd (private communication).

[31] E. M. Lifshitz and L. P. Pitaevskii, *Physical Kinetics* (Pergamon, Oxford, 1981).